scientific reports

Check for updates

OPEN

# Optimisation of the crystallisation process through staggered cooling in a nonvibrating granular system

A. Escobar[1], R. E. Moctezuma[2] & F. Donado[1]✉

**We study experimentally the optimisation of the crystallisation process through a 2D-dimensional system of magnetic particles under an oscillating magnetic field. The time-dependent magnetic field fluidises the system, and by varying its magnitude, the effective temperature of the system is controlled. The system exhibits fluid-like behaviour when the effective temperature is high and evolves to a crystalline arrangement when the temperature is slowly lowered in linear cooling. We found that replacing the linear cooling path with a staggered one let us find the conditions to crystallise the system quicker than using linear cooling. We determine the minimum time required for the particles to find their minimum energy configuration at each temperature step. We found that the crystallisation time was considerably reduced using this method, which allowed us to optimise the crystallisation time.**

**Keywords** Crystallisation process, Cooling profile, Nonvibrating granular system

The solidification process of a fluid using a controlled cooling profile is a fundamental issue both from scientific and technological points of view. Solidification can result in a glass, a crystal, or a heterogeneous system comprising amorphous and crystalline regions[1–4]. If solidification could be fully understood and controlled, materials with specific magnetic, optical, and electrical properties could be made and used in countless scientific and industrial applications. The study of crystallisation has been a relevant topic for a long time because it is an implicit process in obtaining different materials required for science and technological applications, including even in the food and pharmaceutical industries[5].

Although there is much information on the crystallisation process, direct observation of the motion of atoms or molecules ("particles") as a crystal is formed is still challenging. The required methods to get a spatial and temporal resolution have not yet been developed[6]. Different electromagnetic waves or particle scattering techniques have been used to study crystallisation. However, these methods are indirect by nature, and the information obtained through them is still incomplete. Therefore, it is necessary to use complementary techniques to fully understand the process at the particle level. Different model systems has been used for this purpose: colloids[7–14], granular[15–20], big proteins[21,22], among others. Especially, colloidal and granular systems have been widely useful to make important advances in the dynamics of phase transitions[10,20,23,24] since they can be easily observed by videomicroscopy.

The crystallisation process can occur in different ways and under various conditions; its characteristics define the final crystalline material properties and determine its applications[25]. Some methods used to obtain crystals are based on the control of evaporation, precipitation, or cooling[26]. The method's goal is to modify and control the saturation of the molecules of the crystal-forming fluid since solidification begins when the system reaches supersaturation, which enables the formation of small aggregates of particles that evolve into crystals.

Natural cooling, where the environment thermally cools the system[27], favours the formation of several nucleation centres that do not reach a large size, thus giving, as a result, the formation of polycrystals. A linear cooling process, where the temperature gradually decreases, constantly increases the supersaturation. However, the particles do not aggregate at the same rate, so the supersaturation is not controlled. This also leads to the production of crystals that present some polydispersity, although to a lesser degree than in natural cooling.

A programmed cooling[28], composed of two linear coolings intercalating a steady stage at a constant temperature, gives crystals with less polydispersity than for the cases of natural or linear coolings. Different works have been carried out focused on finding the optimal conditions that favour the formation of larger crystals and with better morphology[29,30].

[1]Instituto de Ciencias Básicas e Ingeniería, Universidad Autónoma del Estado de Hidalgo, 42184 Mineral de la Reforma, Hidalgo, México. [2]Conacyt- Instituto de Física, Universidad Autónoma de San Luis Potosí, Álvaro Obregón 64, 78000 San Luis Potosí, S.L.P., México. ✉email: fernando@uaeh.edu.mx

To obtain crystals and optimised crystallisation time, we need to improve the cooling methods, and for that, we need a detailed knowledge of the crystallisation process at the particle level. However, direct observation of the crystallisation process requires very sophisticated methods to meet the size of the particles and the temporal resolution needed. Thus, how can we shed light on the details that occur at the particle level? Macroscopic models such as colloids and granular matter have been used to obtain information about solidification[18,19,31,32]. Glass transition and crystallisation have been studied using these model systems. These models present the advantage that direct observation at the particle level is possible because of the slow dynamics and because particles are easily tracked by standard microscopy. Therefore, crystallisation can be observed in these systems by varying physical quantities such as particle concentration, temperature, and inter-particle interactions.

We used a granular magnetic system under an alternating magnetic field to model crystal and glass-forming fluids in previous works[20,33–36]. In Refs.[20,36], we used linear cooling and examined in detail the initial formation of the nucleus. We have observed that nucleation occurs, in most cases, in a two-step mechanism. In the beginning, a disordered particle aggregate is formed as a first step. In the second step, the aggregate is rearranged by interacting with the wandering non-aggregated particles. In those experiments, we used slow cooling to ensure crystalline formation. For quicker cooling, we obtained disordered or mixed particle configuration. The experiments started in a state of effective high temperature (66 G), which gradually decreased at a rate of 0.02 G / s until the particles reached a state of dynamic arrest (28 G)[36].

The present study seeks to optimise the crystallisation process by configuring the cooling protocol. Instead of cooling following a linear path, we use staggered cooling, where the temperature decreases in large steps, height-steps (the method includes several steps), and the time the system remains at a constant temperature, width-step, is varied to find the minimum time the system crystallises. We carry out various combinations of decreasing height-steps and width-steps to find the condition to optimise the crystallisation time.

Our system is based on an ensemble of 131 steel balls of 1 mm in diameter magnetic particles settled on a concave lens of -250 mm focus length and 50.8 mm in diameter in the middle of a Helmholtz coil arrangement, Fig. 1a, under an alternating magnetic field, $B = B_0 \sin(2\pi f t)$, which randomises particle motions[36]. Each particle takes potential magnetic energy from the magnetic field and transforms it into kinetic energy. This transformation occurs when the particle tries to align with the direction of the magnetic field. It rotates, and because it is settled on the surface, rolls, acquiring kinetic energy. The spherical particle shape contributes to the randomising of the motion because of its neutral equilibrium, Fig. 1b. Thus, the effective temperature, the average of the kinetic energy, is controlled by the intensity of the magnetic field. Because the effective temperature is proportional to the magnetic field amplitude, we characterise the effective temperature with the magnetic field amplitude[33]. The confinement imposed by the lens produces an effective pressure in the system, which is the conjugate variable of the effective area occupied by the particles[20]. Varying the cooling protocol, we found conditions to obtain crystalline final particle configurations, Fig. 1c.

Local parameters characterised the structural evolution. For each particle, is determined the number of nearest neighbours $N$ by using Delaunay triangulation, the closest neighbours the particle is in contact with $N_B$, the sixth orientational order parameter $\psi_6$, see Methods section, and the sixth-bond orientational order parameter $\psi_6'$ which is calculated only considering the $N_B$ particles. A particle surrounded by neighbours in

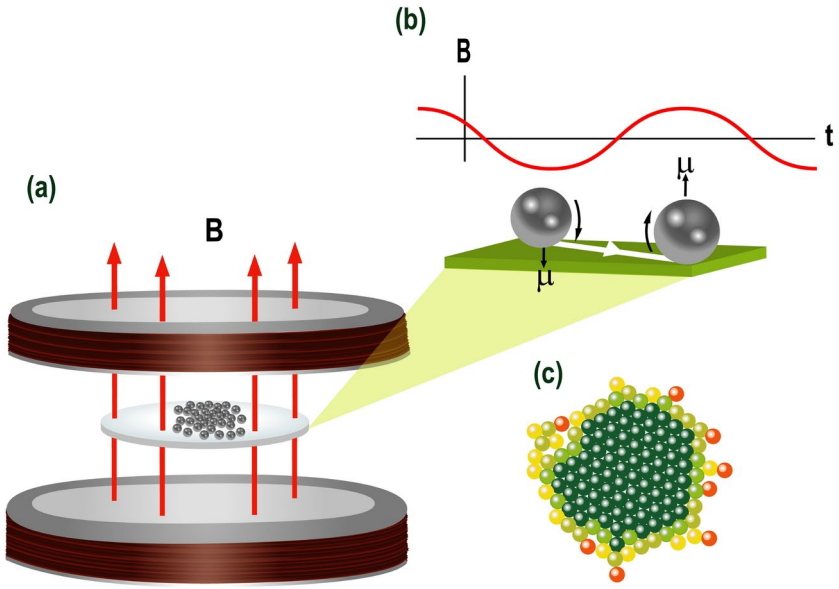


**Fig. 1**. (**a**) The experimental setup consists of magnetic particles in a shallow concave surface (diameter 55 mm) in the middle of Helmholtz coils (inner diameter 152 mm, outer diameter 179 mm). (**b**) A sinusoidal input signal applied into a power amplifier produces an alternating magnetic field. The spherical particles have permanent magnetic dipoles and the variable field makes them roll on the surface in random directions. (**c**) One example of crystalline final particle configuration.

a hexagonal configuration has $\psi_6 = 1$. A value lower than 1 corresponds to the disordered case or simply to a different arrangement from the hexagonal one.

## Crystallisation time optimisation

We carried out experiments at different staggered cooling profiles. For each step-height we varied the step-width to determine the minimum step-width for which the system crystallised. The step-width is the time the system remains at the temperature reached after the sudden quench of a step-height magnitude. In Table S1, see in Supplementary material, provided along with this manuscript, we report the maximum step-width case where the system does not crystallise and the minimum step-width case where the system crystallises for each step-height we used. The first experiment, E1, corresponds to the case of the linear cooling profile. This case was obtained from previous work in a series of experiments where we varied the cooling rate[35]; it was observed that for lower cooling rates, the system crystallises, and for higher cooling rates, the system shows disordered or mixed configurations. The time each case we studied in our present work takes to crystallise is also shown.

Figure 2a shows the cooling profiles for the cases that crystallised in a minimum time for each step-height series studied here. The absolute value of the slopes, $|m|$, is more extensive in the profiles where the crystallisation occurs faster. Figure 2b and c show the final configuration for two cooling profiles having the same step-height but different step-width. Figure 2d shows the data from Table S1, see in Supplementary material. Symbols are coloured according to their average cooling rate. Here, we observe that the greater the slope, the shorter the crystallization time, and this behaviour fits well to a sigmoidal growth function. Two regions are observed; the upper one indicates the appropriate combinations of step-width and step-height to promote crystallisation. Meanwhile, the lower region shows the corresponding combinations that produce amorphous or a combination of amorphous and crystalline phases. Determining the maximum value of the derivative of the sigmoid function, we found the step-height and step-width for which the crystallisation time is the minimum, which occurs for a step of 5.83 G and a waiting time of 45 s, Fig. 2e. Experimentally, we have found that the minimum crystallisation time is reached at a height step of around 4.5 G and a waiting time of 60 s. Even though both values are not the same, the maximum value shown in the curve of the derivative is important, as optimal conditions exist to minimise the crystallisation time.

We have observed that at values higher than the step-heights we studied, the system rapidly solidifies in an amorphous configuration. It needs to be clarified whether it could crystallise if we wait enough time.

Here, we consider only step-height values for what crystallisation occurs. When the step-height the time required for the particles to rearrange in each stage is large, the step-width is large, thus increasing the crystallisation time. If the step-height and step-width are short, the number of cycles to reach the ordered configuration increases, thus also increasing the crystallisation time. Therefore, we observe that intermediate values of step-height and step-width minimize the crystallisation time.

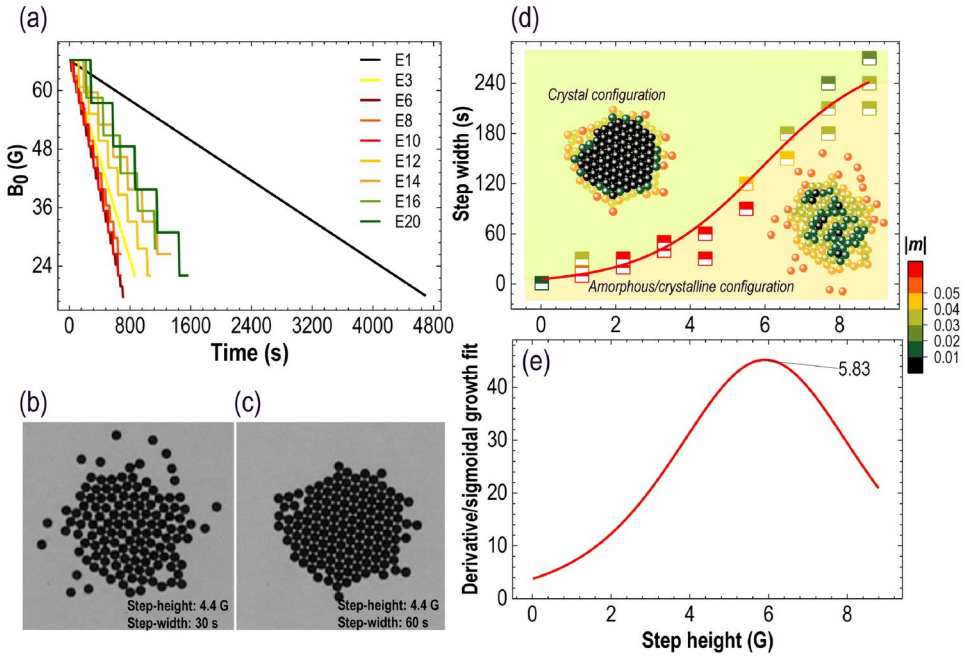


**Fig. 2**. (**a**) Cooling profiles of the cases that crystallised in a minimum time for each step-height series studied here. (**b**) and (**c**) show the final configuration for two different profiles having both a step-height of 4.4 G and a step-width of 30 s and 60 s respectively. (**d**) The slopes of the profiles shown in (**a**) fit well with a sigmoid function and some extra points are added where the system crystallised but the step width is not optimal. (**e**) Derivative of the sigmoid function. The higher value of the curve indicates the optimal value of the step height to minimise the crystallisation time.

In our cooling process, crystallisation depends mainly on the intensity of the magnetic field. The formation of a nucleus occurs within a range of magnetic field values where the energy is low enough for the particles to explore positions of minimum energy and remain close to them.

## Two-step nucleation process

At high temperatures, particles span most of the observation cell, see Fig. 3a. When the temperature decreases, particles interact more frequently. Because of dipolar interactions and the effective pressure over the particles due to the curved surface, particle concentration increases in the centre of the lens. The formation of a nucleus begins with a stable aggregate formed when an ensemble of particles falls in a configuration of local minimum energy, see Fig. 3b. This aggregate is amorphous, and although it could contain some ordered tiny grains, the entire aggregate is disordered. This aggregate experiments a rearrangement by its interactions with the wandering free particles surrounding the aggregate and by magnetic interactions between them and the field. At the same time, the aggregate continues growing. New particles can be attached to it in two ways: individually or in small groups. The nucleus's formation ended when the aggregate's central part was ordered; see Fig. 3c. Finally, the particles have formed a single crystal, as shown in Fig. 3d. This process follows the two-step mechanism theoretically proposed in the literature and is supported by some other experimental studies, see Refs.[20,37,38].

The growth of the crystal occurs in a similar fashion: first, shells in disordered configuration around the nucleus form, and then they are reordered by the effective interaction with the magnetic field and the pressure of the free wandering particles. We will discuss this process in detail in the next section.

Figure 4 shows images of configurations at different stages obtained from different cooling profiles. The appearance of the nucleus occurs when the magnetic range is between 50 G and 40 G. All the final configurations shown in Fig. 4 are crystalline with similar shapes with ordered particle configurations in the hexagonal close-packed arrangement. We can observe in Fig. 4, in the rectangle highlighted in yellow, photographs where a nucleus is formed in each series. It is observed that particles in the periphery are in disordered configurations. As the crystal grows in each experiment, as the temperature decreases, the periphery becomes ordered and part of the crystal while a concentric new disordered periphery forms.

The case of step-height of 4.4 G was studied in more detail at two step-widths: one when the system did not crystallise, the case with the larger step-width without crystallisation and one that it does, the case with the shorter step-width when crystallisation occurs. In Fig.2b and c, are shown the corresponding two final particle configurations. The analysis of the aggregates was characterized by using the following parameters: packing fraction $\phi_{2D}$, the average sixth-bond orientational order parameter $\bar{\psi_6'}$, number of particles conforming to the aggregate $N$, and the number of particles with five and six bonded neighbours. In Fig. 5 we show the evolution of the structure of the system in the cases with and without crystallisation.

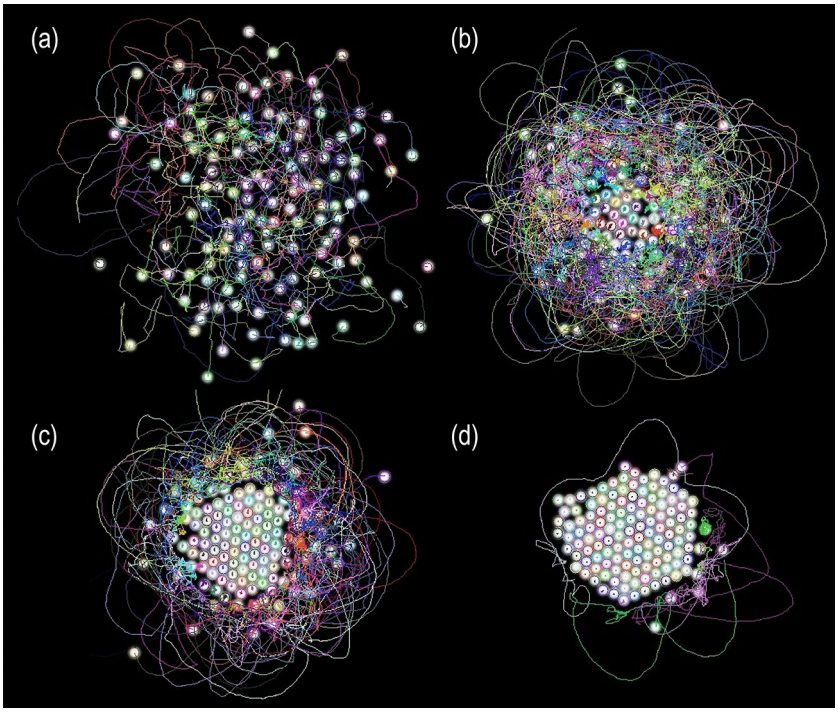


**Fig. 3**. Evolution of the structure for the case of step-height 4.4 G and step-width 60 s. (**a**) Trajectories span all the surface, (**b**) Formation of an amorphous aggregate, (**c**) Re-arrangement of the central aggregates and formation of an amorphous layer around an ordered nucleus, (**d**) Formation of an ordered aggregate with a few particles around.

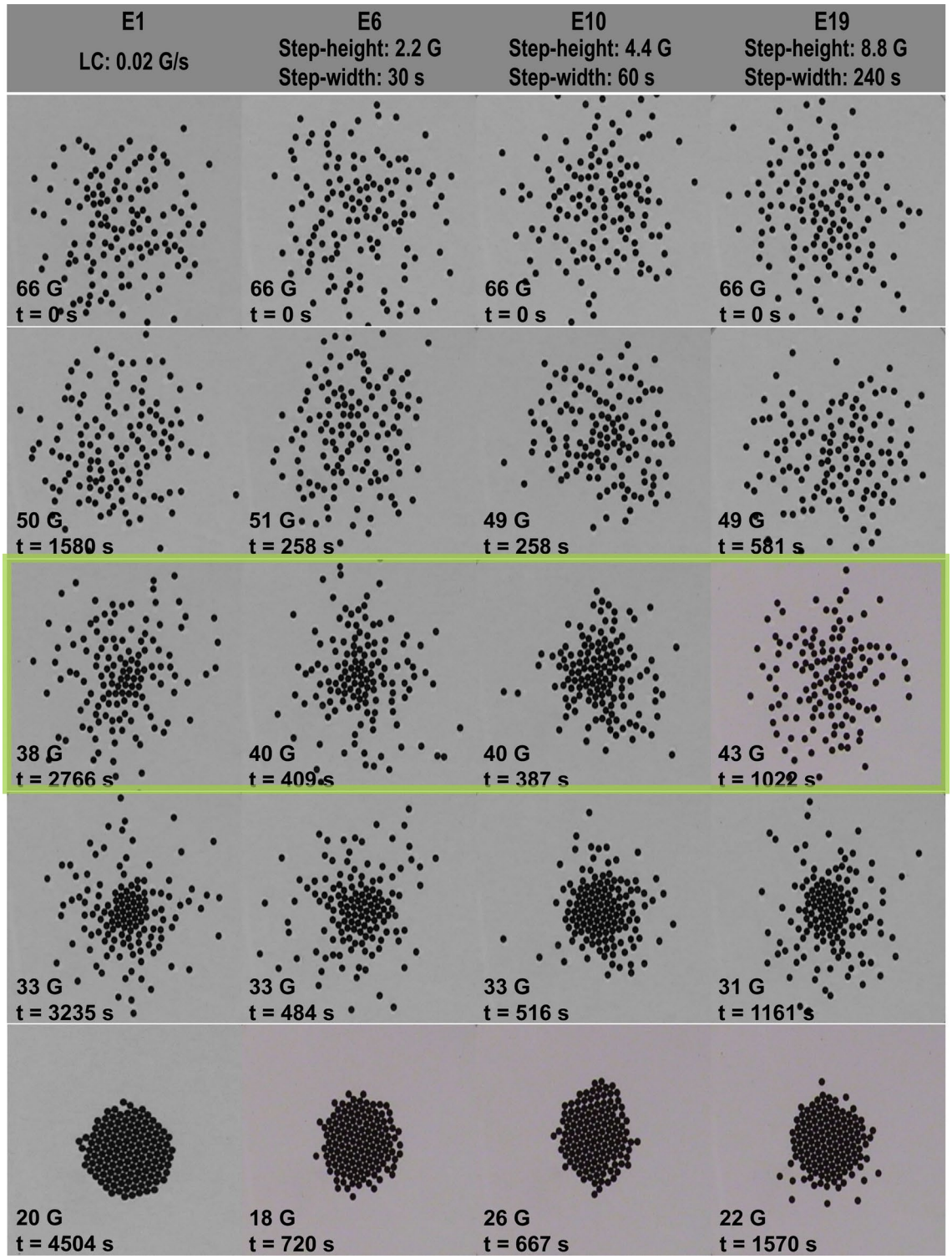


**Fig. 4**. Structures formed at different stages in four different experiments. In the first column, we have the case of linear cooling (E1). The next three columns correspond to experiments with a step-height where the system crystallises in the shortest time (E6, E10, and E19). The row marked in green shows the stage where the formation of the nucleus begins.

It is observed that the packing fraction shows rises and falls that coincide with each step-height change after a step-width at a constant temperature.

In the case of a step-height of 4.4 G (Fig. 5), we observe that the packing factor when the system does not crystallise oscillates around 50%, Fig. 5a, and around 70% when it does crystallise, Fig. 5b, which means that at the beginning, if the packing fraction is lower than a threshold the crystallisation may no reaches. In both cases, the sixth-bond

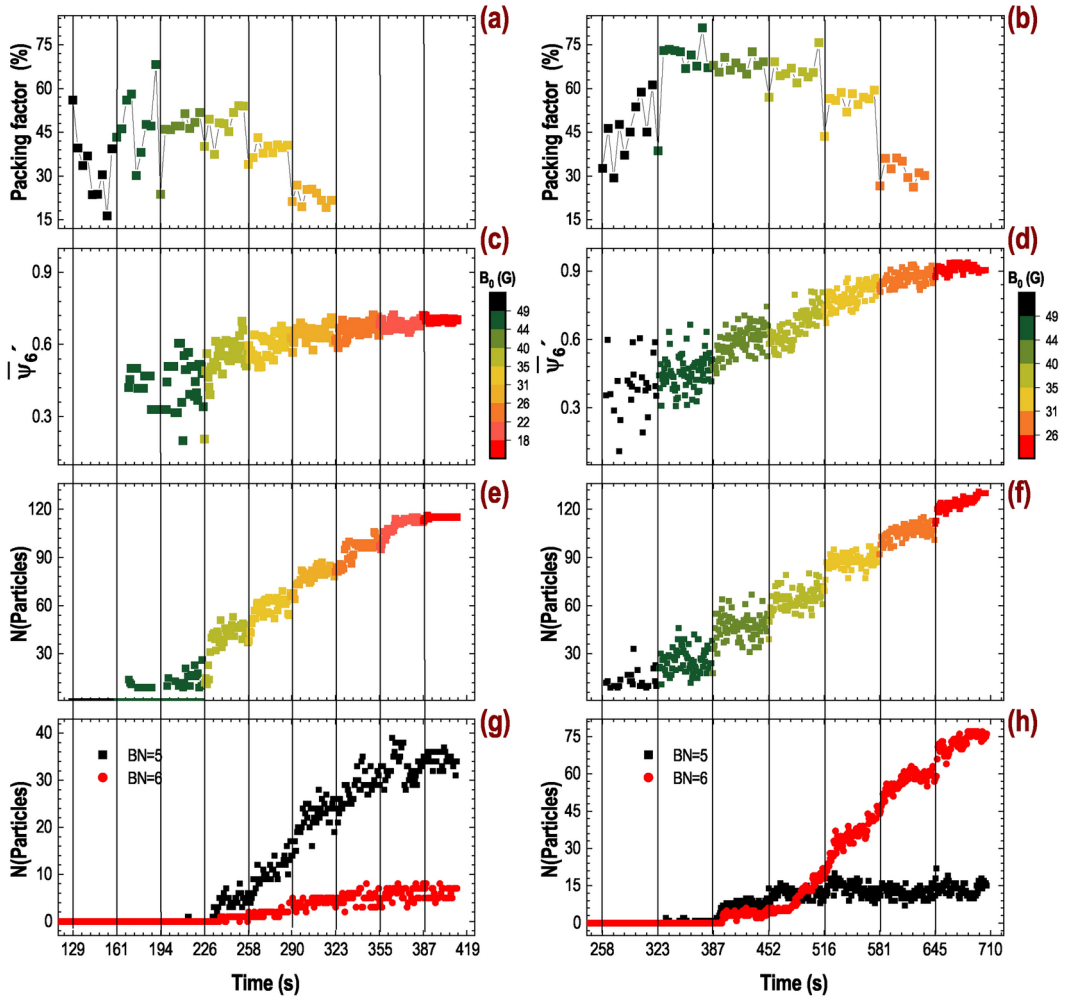


**Fig. 5**. Evolution of the structure in time, using a step-height of 4.4 G and step-widths of (**a,c,e,g**) 30 s, where the system did not crystallise, and (**b,d,f,h**) 60 s, when it did. The first row from the top is the packing factor (**a,b**), the second row is the average sixth-bond orientational order parameter $\bar{\psi}_6'$ (**c,d**), the third row is the number of particles forming the aggregate (**e,f**), and the last row is the number of particles with five and six bonded neighbours (**g,h**).

orientational order parameter, $\bar{\psi}_6'$, grows slowly in each stage, and the overall curve presents an almost continuous increase. For a step-width of 30 s, the values remain below 70% (c), indicating that the system is in disorder. On the other hand, for a step-width of 60 s, this value exceeds 90% (d), meaning the system is almost in a hexagonal arrangement. In Fig. 5e and f, the size of the aggregate over time is shown; as cooling occurs, the number $N$ of adhered particles grows. In these graphs, discontinuous curves are observed; the continuous regions corresponding to each stage where the temperature remains constant are observed. When the step-width is 60 s (f), the plateaus are clearer since the particles had more time to take their minimum energy positions, and the system reached a stationary state before the temperature decreased again. For the case where there was no crystallisation (e), the increase of particles stopped before that in the case that crystallises, and the plateaus did not reach a stationary state.

Interestingly, the main difference between the two experiments is observed in the curves showing the number of particles with five and six neighbours in contact with a determined particle. In the disordered system Fig. 5g, the number of particles with five neighbours increases significantly. In comparison, the number of particles with six neighbours has a slight increase and remains below ten particles in the aggregate. In contrast, when the structure reaches order, see Fig. 5h, both values increase similarly. However, the curve with five neighbours is slightly higher until around 35 G (temperature in which the central aggregate is already consolidated). At this point, it is observed that the curve of particles depicting six neighbours rises more rapidly, and the curve of particles with five neighbours remains almost constant, although the crystal is quickly growing. An inversion of the particle populations is observed, which determines the point at which the nucleus is consolidated.

## Packing factor role in the crystallisation

Until now, we have observed that both the structural and dynamic parameters in the system evolve in plateaus, which coincide with the periods in which the temperature changes from one step to another. Each plateau shows

how, as the temperature decreases, the concentration increases, forming a layer of amorphous particles between the centrally ordered aggregate and the free particles. This layer becomes ordered as time goes on due to the collisions of the outermost particles. At some point, the saturation decreases, and another jump in temperature is necessary for particle adhesion to continue. This behaviour is characterised by the packing factor of the adhesion layer in each plateau (see Methods section). We use the cases with step-height of 4.4 G, with three step-widths 90 s, 60 s and 30 s for comparisons. In the diagram of Fig. 6a, we depict the relationship between the fraction of area occupied by the particles and the magnetic field once the particles started to aggregate ($\sim$ 40G). For the step-width of 30 s, a packing factor below 70% was obtained. It indicates that, although sufficient concentration was generated to make the particles aggregate, the waiting time was not ideal for reaching the ordering stage. The highest packing efficiency was reached when the step-width was 60 s, with an average above 75%. Here, the concentration and the time in which the energetic conditions were maintained to achieve the aggregation and the crystalline structure were adequate. In the third experiment, the temperature remained constant for a longer time (90 s), and the packing factor was similar to the second case, with an average above 70%.

Figure 6 shows coloured regions in each graph. In the lower region (in orange), the particle concentration is below than the necessary to form stable aggregates so that it could be seen as an unsaturated region. The intermediate region (in yellow) could be considered the metastable zone, where growth is more likely to occur. The concentration is even higher in the upper region (in green), indicating that the system gets ordered. An optimum supersaturation above 70% must be reached at each plateau for the adhesion layer to form. When the temperature remains constant, the saturation has to be maintained in the intermediate zone, allowing the particles to be reorganised. Once the saturation is exhausted, the drop in temperature again generates supersaturation, and the cycle is repeated until the crystal is formed. Figure 6b shows areas shaded in red, which indicate the area fraction used to determine the packing factor in each region.

Our results show that the structural parameters evolve synchronously with temperature drop changes. In each step, it can be seen how, as time goes on, the concentration increases, forming a layer of amorphous particles between the central aggregate and the free particles, which becomes ordered due to the collisions of the external free particles. The particles search for minimum energy configurations by exploring the surface; they can find it if they have enough time. At some point, the saturation decreases, and another drop in temperature is needed

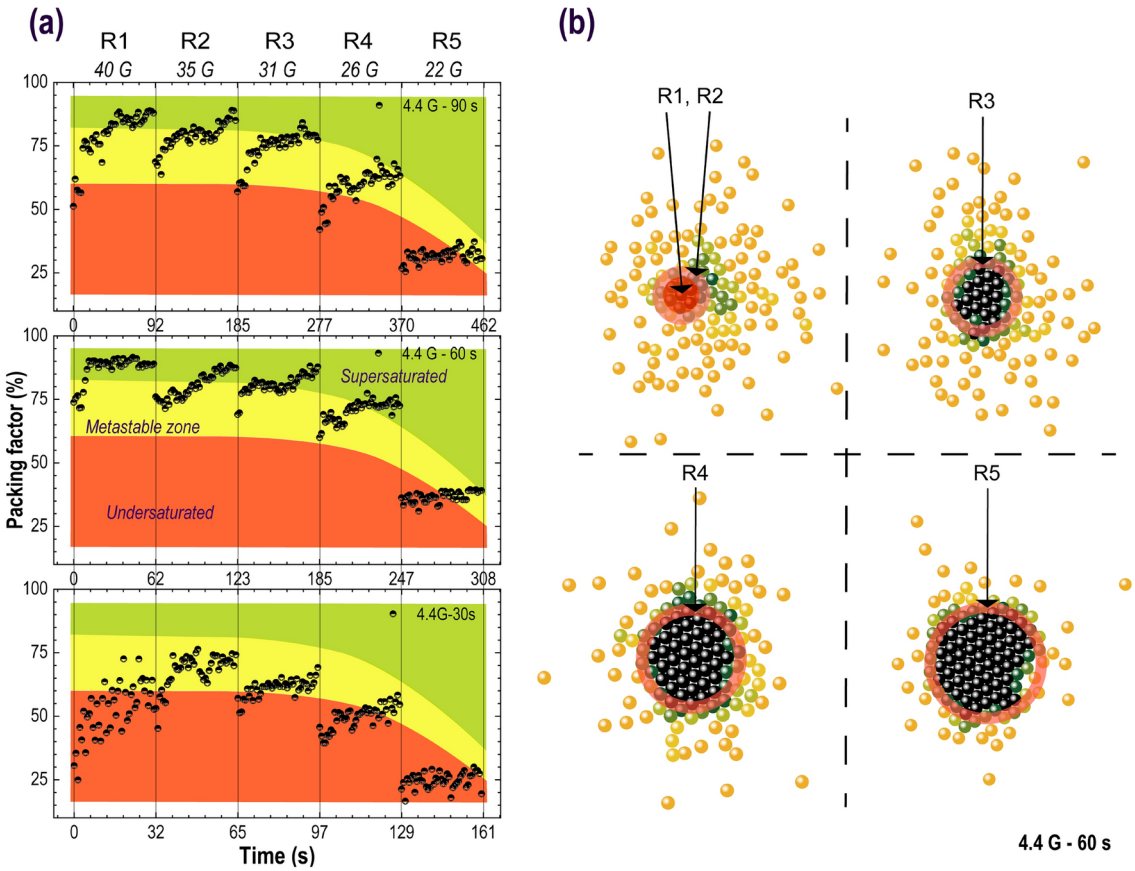


**Fig. 6**. (**a**) Packing factor for the case where a step-height of 4.4 G and three step widths were used; 30 s (does not crystallise), 60 s (crystallises), and 90 s (crystallises). Each colour depicts the saturation regions during the cooling process: the undersaturated region in orange, the intermediate or metastable region in yellow, and the supersaturated region in green. (**b**) The shaded regions indicate the area fraction used to calculate the packing factor throughout the cooling.

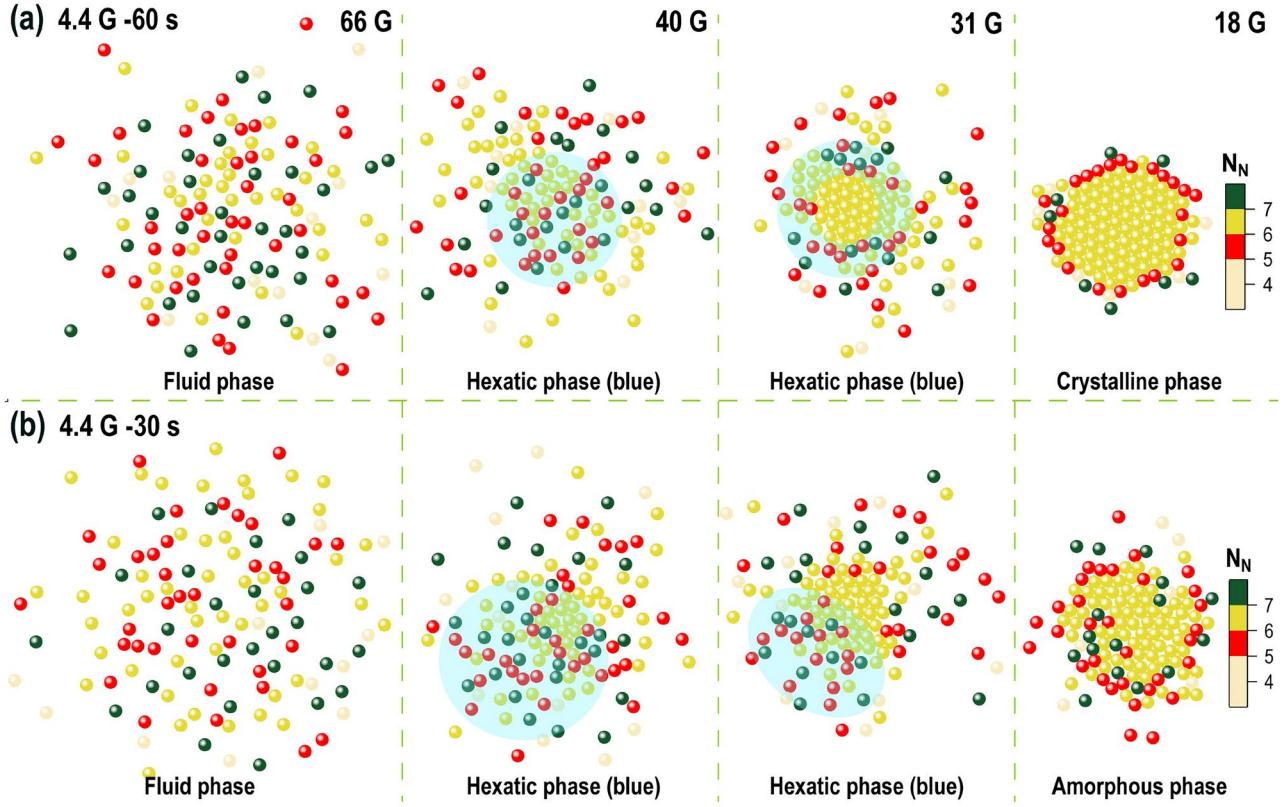


**Fig. 7**. Identification of the hexatic phase throughout the cooling process with the step-height of 4.4 G and two different widths 60 and 30 seconds, where the system crystallises and where it does not. The particles are coloured according to the number of nearest neighbours $N_N$, and the shaded region depicts the hexatic phase.

for particle aggregation to continue. Thus, there is an optimal concentration to form the amorphous layer and its subsequent ordering. The impact of step-width on the process is profound. If the step-width is too short, the optimal concentration remains elusive, and further ordering becomes impossible. Conversely, if the step-width exceeds the optimal range, the crystallisation time significantly lengthens.

In the last stages of the solidification, we observed that the corresponding R4 and R5 regions do not meet the criteria described in this section, even though the system crystallised. We observed that no additional layer of particles surrounds this region. Particles adhere to the crystal following a more direct path, following a classical mechanism.

## Hexatic-like phase

The crystallisation process is, in a certain way, the inverse of the melting process; both processes share some aspects. Thus, some attempts have been made to use melting theories to explain crystallisation with a wide degree of success. In particular, in 2D systems, the KTHNY theory, developed in the context of melting, has been used to describe crystallisation. This theory emphasises the role of topological defects and grain boundaries in describing melting, proposing a two-step mechanism that includes the formation of an intermediate phase called hexatic phase[39,40]. The phase transition dynamics can be explained in terms of the creation and dissociation and the binding and unbinding of topological defects, such as disclinations and dislocations. A disclination is a particle with five or seven neighbours; a dislocation is a pair of disclinations, one with five and one with seven neighbours[40,41]. In brief, the melting process starts with creating pairs of dislocations due to thermal fluctuations. When the pairs are disassociated, when there is an abundance of free dislocations, we have the hexatic phase; this is the first step of the melting. In the second step, we obtained the fluid phase when dislocations are disassociated to give free disclinations. Therefore, a footprint of the hexatic phase is the abundance of dislocations.

In this work, we have focused on finding the conditions to optimise the crystallisation time. Our results agreed that nucleation is a two-step nucleation process, where an amorphous structure mediates the transition from fluid to crystal. We analysed this amorphous structure to look for the existence of a hexatic-like phase by identifying disclinations and dislocations. Figure 7 shows two series of particle configurations: a case where a final crystalline configuration was reached, Fig. 7a, and a case where the final ordered configuration was not reached Fig. 7b. In the figure, particles coloured in green are disclinations of seven neighbours, red particles are disclinations of five neighbours, and the yellow particles are particles with six neighbours. In Fig. 7a, disclinations are unbounded in the configuration at 66 G, as expected for the fluid phase. At 40 G, a region where dislocations, pairs of disclinations, can be observed has been highlighted in blue. This small region can

be identified as a hexatic phase. At 31 G, the nucleus has formed, and now a region of hexatic phase is formed around the nucleus. Finally, for 18 G, an ordered crystalline configuration is reached. We highlighted hexatic phase regions in Fig. 7b. However, the number of unbounded disclinations, the low number of dislocations, and the quick cooling prevent the system from ordering. For the case of a step-width of 30 s, 7b, the time the system remains at an effective temperature is not enough to let the particles reorder, letting the disclinations join to form abundant dislocations. In contrast, in the step-width of 60 seconds, there is enough time for the formation of abundant dislocations, which in the reordering process, disappear to give rise to an ordered region with crystalline order. Rapid cooling does not allow the system to reach the local particle concentration necessary to promote the formation of dislocations and then the ordering. Interestingly, we have found that the critical particle concentration to promote ordering is around 70%. In Ref.[39], a study of 2D melting simulations, it was shown that if the concentration does not exceed the value of 70%, the hexatic phase and later the ordered phase are not reached. This opens up the possibility of further studying the feasibility of using melting theory in the crystallisation process in this system.

## Conclusions and outlook

We have shown that a staggered cooling profile notably affects solidification, allowing the system to crystallise (or not) and affecting the solidification time. Each step-height case has a minimum step-width that enables the system to crystallise. Finding the proper values in the step-height and step-width allows the system to have the appropriate conditions in which the crystallisation time is optimised.

In terms of the two-step crystallisation theory, a staggered cooling protocol favours the formation of an amorphous layer of particles when the temperature drops in the first step, and then in the second step, the particle configuration evolves toward a more ordered configuration.

If the local particle concentration in a molecular crystal-forming liquid could be tracked in real-time, our studies suggest practical methods to control and optimise crystallisation time. We could drop the effective temperature very fast to reach values in the metastable region, then keep the temperature until the reorganisation is observed and the particle concentration is around 77 %.

## Methods

### Packing fraction

The packing fraction is characterised by the fraction of area occupied by the particles; this is defined as follows;

$$\phi_{2D} = \frac{n \cdot A_p}{A_T},$$

where $n$ is the number of particles in an area $A_T$, $A_p$ is the occupied area of one particle. For arbitrary fringes, however, we need to account that the fringe could contain fractions of particles and that the $A_T$ correspond to a circular fringe. To calculate the packing fraction in our system, we made a digital treatment of the frame to obtain a binary image where the particles are seen as dark circles. We obtained the intersection of the circular fringe with the binary image and determined the total area occupied by particles and portions of the particles inside the fringe. The area of the fringe is determined as a subtraction of areas of the circles that formed the fringe. Then, we calculate the ratio between the area occupied by the particles in a given fringe and the area of the corresponding fringe. We give the values of the packing fraction as a percentage obtained by multiplying the fraction of the area occupied by the particles by 100. The maximum packing fraction of a compact hexagonal arrangement is expected to be 91 %. This parameter is a useful structural measurement to characterise how compact the particle configuration is.

### Effective temperature

In our system, the magnitude of the alternating magnetic field plays the role of an effective temperature. The connection between these two parameters is discussed in detail in Ref.[42]. In that work, it is shown that the energy input $U$ is proportional to the frequency and amplitude of the unsteady part of a magnetic field, $B_0 \sin(2\pi f t)$,

$$\left\langle \frac{dU}{dt} \right\rangle = 4\mu B_0 f. \tag{1}$$

Because of the friction of particles and the surface container and collisions between particles, not all the available energy, $4\mu B_o f$, is transformed into the particle kinetic energy. Although energy is quickly lost, it is compensated by the continuous energy input coming from the unsteady magnetic field. This energy input prevents particle motions from stopping. Thus, even though the system is not in thermodynamic equilibrium, but in a stationary state, the statistical mechanics tools developed for equilibrium systems can be used[43]. On the other hand, the effective temperature can be calculated using the equipartition theorem for 2D systems,

$$\left\langle \frac{1}{2} m v^2 \right\rangle = T_E,$$

where the Boltzmann constant is set as $k_B = 1$ (as in vibrating granular systems). Since the effective temperature is proportional to kinetic energy, which is proportional to $B_o$ when the frequency is kept constant, the effective temperature is proportional to $B_o$. In this work, we used $B_o$ as the effective temperature.

### Orientational order parameter

The Delaunay-Voronoi plugin in ImageJ was used to generate the Delaunay triangulation, from which, for each particle *j*, the nearest neighbour $N_j$ positions were determined. Some of the nearest neighbours might be in contact with, but some of them may not, even if they are the closest. To determine the number of neighbours linked or in contact, also known as the coordination number $N_{jB}$, a cutoff distance of 1.1 $\sigma$ is used as a cutoff criterion ($\sigma$ is the diameter of the particle). Neighbouring particles closer than the cutoff distance are counted in the number of linked neighbours $N_{jB}$. Based on the information of the nearest neighbours $N_j$, the orientational parameter $\psi_6^j$ was calculated for each particle *j*, which is defined as:

$$\psi_6^j = \frac{1}{N_j}\left|\sum_{k=1}^{N_j} \exp(\mathrm{i}\,6\theta_{jk})\right| \tag{2}$$

where the sum on *k* is over the $N_j$ neighbours of particle *j* and $\theta_{jk}$ is the angle formed between the *x*-axis and the vector pointing from *j* to *k*.

## Data availibility

The authors declare that the data supporting the findings of this study are available within the paper, its supplementary information files.

Received: 2 July 2024; Accepted: 23 December 2024
Published online: 06 January 2025

## References

1. Ediger, M. D., Angell, C. A. & Nagel, S. R. Supercooled liquids and glasses. *J. Phys. Chem.* **100**, 13200 (1996).
2. Debenedetti, P. G. & Stillinger, F. H. Supercooled liquids and the glass transition. *Nature* **410**, 259 (2001).
3. Stevenson, J. D. & Wolynes, P. G. The ultimate fate of supercooled liquids. *J. Phys. Chem. A* **115**, 3713 (2011).
4. Sosso, G. C. et al. Crystal nucleation in liquids: open questions and future challenges in molecular dynamics simulations. *Chem. Rev.* **116**, 7078 (2016).
5. Yu, L. & Reutzel-Edens, S. M. Crystallisation - basic principles. *Encycl. Food Sci. Nutr.* **88**, 1697–1702 (2002).
6. König, H. Elementary triangles in a 2D binary colloidal glass former. *Europhys. Lett.* **71**, 838 (2005).
7. Pusey, P. N., Van Megen, W., Underwood, S. M., Bartlett, P. & Ottewill, R. H. Colloidal fluids, crystals and glasses. *Physica A* **176**, 1 (1991).
8. Murray, C. A. & Grier, D. G colloidal crystals. *Am. Sci.* **83**, 3 (1995).
9. Habdas, P. & Weeks, E. R. Video microscopy of colloidal suspensions and colloidal crystals. *Curr. Opin. Colloid Interface Sci.* **7**, 3 (2002).
10. Anderson, V. J. & Lekkerkerker, H. N. Insights into phase transition kinetics from colloid science. *Nature* **416**, 6883 (2002).
11. Deutschländer, S., Horn, T., Löwen, H., Maret, G. & Keim, P. Two-dimensional melting under quenched disorder. *Phys. Rev. Lett.* **111**, 259901 (2013).
12. Chen, J. S. Grand challenges for colloidal materials and interfaces: dancing on nano-stage. *Front. Mater.* **1**, 1 (2014).
13. Hensley, A., Videbæk, T. E., Seyforth, H., Jacobs, W. M. & Rogers, W. B. Macroscopic photonic single crystals via seeded growth of DNA-coated colloids. *Nat. Commun.* **14**, 4237 (2023).
14. Solano-Cabrera, C. O. et al. Self-assembly and transport phenomena of colloids: confinement and geometrical effects. *Annu. Rev. Condens. Matter Phys.* **16**, 041124 (2024).
15. Amirifar, R., Dong, K., Zeng, Q. & An, X. Self-assembly of granular spheres under one-dimensional vibration. *Soft Matter* **14**, 14 (2018).
16. Blair, D. L. & Kudrolli, A. Clustering transitions in vibrofluidized magnetized granular materials. *Phys. Rev. E* **67**, 2 (2003).
17. Daniels, K. E. & Behringer, R. P. Hysteresis and competition between disorder and crystallization in sheared and vibrated granular flow. *Phys. Rev. Lett.* **94**, 16 (2005).
18. Rietz, F., Radin, C., Swinney, H. L. & Schröter, M. Nucleation in sheared granular matter. *Phys. Rev. Lett.* **120**, 055701 (2018).
19. Reis, P. M., Ingale, R. A. & Shattuck, M. D. Crystallization of a quasi-two-dimensional granular fluid. *Phys. Rev. Lett.* **96**, 258001 (2006).
20. Escobar, A., Ledesma-Motolinía, M., Carrillo-Estrada, J. L. & Donado, F. Two-step crystallisation in a 2D active magnetic granular system confined by a parabolic potential. *Sci. Rep.* **13**, 8552 (2023).
21. Vekilov, P. G. & Alexander, J. I. D. *Chem. Rev.***100**, 6 (2000).
22. Zhang, F. Nonclassical nucleation pathways in protein crystallization. *J. Phys. Condens. Matter* **29**, 44 (2017).
23. Li, B., Zhou, D. & Han, Y. Assembly and phase transitions of colloidal crystals. *Nat. Rev. Mater.* **1**, 15011 (2016).
24. Bonilla-Capilla, B., Ramírez-Saito, A., Ojeda-López, M. A. & Arauz-Lara, J. L. Hydrodynamic interactions between colloidal particles in a planar pore. *J. Phys. Condens. Matter* **24**, 464126 (2012).
25. Tegze, G., Gránásy, L., Tóth, G. I., Douglas, J. F. & Pusztai, T. Tuning the structure of non-equilibrium soft materials by varying the thermodynamic driving force for crystal ordering. *Soft Matter* **7**, 1789–1799 (2011).
26. Mersmann, A. Crystallization and precipitation. *Chem. Eng. Process.* **38**, 345 (1999).
27. Tavare, N. S. Batch crystallizers. *Rev. Chem. Eng.* **7**, 211–355 (1991).
28. Mullin, J. W. & Nývlt, J. Programmed cooling of batch crystallizers. *Chem. Eng. Sci.* **26**, 369–377 (1971).
29. Jones, A. G. Optimal operation of a batch cooling crystallizer. *Chem. Eng. Sci.* **29**, 1075 (1974).
30. Jones, A. G. & Mullin, J. W. Programmed cooling crystallization of potassium sulphate solutions. *Chem. Eng. Sci.* **29**, 105 (1974).
31. Cafiero, R., Luding, S. & Herrmann, H. J. Rotationally driven gas of inelastic rough spheres. *Phys. Rev. Lett.* **84**, 6014 (2000).

32. Panaitescu, A., Reddy, K. A. & Kudrolli, A. Nucleation and crystal growth in sheared granular sphere packings. *Phys. Rev. Lett.* **108**, 108001 (2012).
33. Tapia-Ignacio, C., Moctezuma, R. E. & Donado, F. Structure and fragility in a macroscopic model of a glass-forming liquid based on a nonvibrating granular system. *Phys. Rev. E* **98**, 032901 (2018).
34. Moctezuma, R. E., Arauz-Lara, J. L. & Donado, F. Structural characterization of a magnetic granular system under a time-dependent magnetic field: Voronoi tessellation and multifractal analysis. *Physica A* **496**, 27 (2018).
35. Escobar, A., Tapia-Ignacio, C., Donado, F., Arauz-Lara, J. L. & Moctezuma, R. E. Glass- and crystal-forming model based on a granular two-dimensional system. *Phys. Rev. E* **101**, 052907 (2020).
36. Escobar, A., Donado, F., Moctezuma, R. E. & Weeks, E. R. Direct observation of crystal nucleation and growth in a quasi-two-dimensional nonvibrating granular system. *Phys. Rev. E* **104**, 044904 (2021).
37. Vekilov, P. G. The two-step mechanism of nucleation of crystals in solution. *Nanoscale* **2**, 2346–2357 (2010).
38. Savage, J. R., Pei, L. & Dinsmore, A. D. Experimental studies of two-step nucleation during two-dimensional crystallization of colloidal particles with short-range attraction. *Adv. Chem. Phys.* **151**, 111–135 (2012).
39. Bernard, E. P. & Krauth, W. Two-step melting in two dimensions: first-order liquid-hexatic transition. *Phys. Rev. Lett.* **107**, 155704 (2011).
40. Vasilieva, E. V. & Vaulina, O. S. Orientational order and formation of topological defects in two dimensional systems. *JETP* **117**, 1 (2013).
41. Vasilieva, E. V., Petrov, O. F. & Vasiliev, M. M. Laser-induced melting of two-dimensional dusty plasma system in RF discharge. *Sci. Rep.* **11**, 1 (2021).
42. Tapia-Ignacio, C., Garcia-Serrano, J. & Donado, F. Nonvibrating granular model for a glass-forming liquid: Equilibration and aging. *Phys. Rev. E* **94**, 062902 (2016).
43. Donado, F., Moctezuma, R. E., López-Flores, L., Medina-Noyola, M. & Arauz-Lara, J. L. Brownian motion in non-equilibrium systems and the Ornstein-Uhlenbeck stochastic process. *Sci. Rep.* **7**, 1 (2017).


## Acknowledgements

Financial support from CONAHCyT, México, through Grants 731759 and C-554/2023 (Ciencia de Frontera) is acknowledged. A.E. acknowledges the postdoctoral fellowship from CONAHCyT, México: Convocatoria 2023(1).

## Author contributions

Author contributions: A. Escobar performed the experiments and analysed the experimental data. R.E. Moctezuma wrote part of the manuscript. F. Donado designed and supervised the experimental research and wrote the final version of the manuscript. All the authors contributed to the discussion of the results.

## Declarations

## Competing interests

The authors declare no competing interests.

## Additional information

**Supplementary Information** The online version contains supplementary material available at https://doi.org/10.1038/s41598-024-84285-4.

**Correspondence** and requests for materials should be addressed to F.D.

**Reprints and permissions information** is available at www.nature.com/reprints.

**Publisher's note** Springer Nature remains neutral with regard to jurisdictional claims in published maps and institutional affiliations.